

# A Global Landslide Non-Susceptibility Map

Guoqiang Jia<sup>a,b</sup>, Massimiliano Alvioli<sup>c</sup>, Stefano Luigi Gariano<sup>c</sup>, Ivan Marchesini<sup>c</sup>, Fausto Guzzetti<sup>d</sup>, Qiuhong Tang<sup>a,b</sup>

<sup>a</sup> Key Laboratory of Water Cycle and Related Land Surface Processes, Institute of Geographic Sciences and Natural Resources Research, Chinese Academy of Sciences, Beijing, 100101, China

<sup>b</sup> University of Chinese Academy of Sciences, Beijing, 100049, China

<sup>c</sup> Research Institute for Geo-Hydrological Protection, Italian National Research Council (IRPI CNR), via Madonna Alta 126, Perugia, 06128, Italy

<sup>d</sup> Italian National Civil Protection Department, via Vitorchiano 2, Rome, 00189, Italy

**Corresponding author:** Massimiliano Alvioli (email: [massimiliano.alvioli@irpi.cnr.it](mailto:massimiliano.alvioli@irpi.cnr.it)); Qiuhong Tang (email: [tangqh@igsnr.ac.cn](mailto:tangqh@igsnr.ac.cn))

**Acknowledgements.** This work is supported by the National Natural Science Foundation of China (Grant No. 41730645), the Strategic Priority Research Program of Chinese Academy of Sciences (Grant No. XDA20060402), and the Second Tibetan Plateau Scientific Expedition and Research (Grant No. 2019QZKK0208). G. Jia was supported by the China Scholarship Council (CSC201904910615) and acknowledged kind hospitality and support of CNR IRPI, Perugia. We further appreciated the three anonymous referees for their valuable comments, which helped us improve our work greatly.

27 **Abstract**

28 At variance with conventional landslide susceptibility assessment, non-susceptibility  
29 analysis aims at selecting locations in which the likelihood of landslide occurrence is  
30 null or negligible. The advantage of this approach is that it does not require estimating  
31 different degrees of likelihood outside of the locations of negligible susceptibility. Thus,  
32 it entails the use of simplified classification methods. In this work, we tested and  
33 validated the existing non-susceptibility model with 18 global and regional landslide  
34 datasets, as a prior for the global application. The existing model was applied previously  
35 in Italy and the Mediterranean region, and defined by a non-linear relief vs. slope  
36 threshold curve, below which landslide susceptibility is negligible. Then, we applied a  
37 similar analysis, and proposed a global map, using relief and slope obtained from global  
38 elevation data at about 90-m resolution. The global map classifies 82.9% of the  
39 landmasses with negligible landslide susceptibility. The non-susceptible areas are  
40 broadly consistent with the “very-low” susceptibility class in existing global and  
41 continental landslide susceptibility maps and a national non-susceptibility map in the  
42 conterminous United States. Quantitative analyses revealed that population and  
43 settlements are denser within non-susceptible area than elsewhere, which makes the  
44 map of potential interest for non-exposure analysis, land planning and disaster  
45 responses at a global scale.

46 **Keywords:** non-susceptibility; quantile non-linear model; validation; non-exposure  
47 analysis

48

49  
50  
51  
52  
53  
54  
55  
56  
57  
58  
59

## **A Global Landslide Non-Susceptibility Map**

Guoqiang Jia<sup>a,b</sup>, Massimiliano Alvioli<sup>c</sup>, Stefano Luigi Gariano<sup>c</sup>, Ivan Marchesini<sup>c</sup>, Fausto Guzzetti<sup>d</sup>, QiuHong Tang<sup>a,b</sup>

### **Highlights**

- We extended and validated an existing non-susceptibility model for landslides
- About 82.9% of the global landmasses are covered by non-susceptible areas
- Results of non-susceptibility analyses vary with regions and landslide types
- The global map is of potential interest for non-exposure analysis, planning and disaster response

# A Global Landslide Non-Susceptibility Map

Guoqiang Jia<sup>a,b</sup>, Massimiliano Alvioli<sup>c</sup>, Stefano Luigi Gariano<sup>c</sup>, Ivan Marchesini<sup>c</sup>, Fausto

Guzzetti<sup>d</sup>, QiuHong Tang<sup>a,b</sup>

## 1. Introduction

Landslide hazard and risk assessment are a relevant scientific and social issues owing to the global impact of slope failures on human activities and natural environment. Recently, global landslide studies are becoming frequent, and efforts have been made to compile global landslide datasets and models applicable to global datasets (Kirschbaum et al., 2010, 2015; Froude and Petley, 2018; Haque et al., 2019). Global maps of landslide susceptibility (Hong et al., 2007a; Farahmand and Aghakouchak, 2013; Stanley and Kirschbaum, 2017), or global landslide hazard and risk assessment (Hong et al., 2006; Kirschbaum et al., 2009; Nadim et al., 2006, 2013) also exist. Rainfall thresholds for landslide initiation at a global scale were proposed (Guzzetti et al., 2008; Hong and Adler, 2008; Jia et al., 2020), as well as global landslide warning systems (Hong et al., 2007b; Kirschbaum and Stanley, 2018). A link between landslide features and climate change, mostly through rainfall data, at a global scale was also investigated (Kirschbaum et al., 2015; Gariano and Guzzetti, 2016; Haque et al., 2019). The reasons for a globally homogeneous landslide analysis are manifold, including: (a) it is useful in data scarce regions, where detailed information is not available (Jacobs et al., 2020); (b) it allows finding similarities and differences in the spatial pattern of landslide occurrence in different settings (Tanyas et al., 2019a; 2019b; Tanyas and Lombardo, 2020); and (c) it provides opportunities for different regions to communicate and compare their disaster prevention and mitigation strategies with a common baseline (Guzzetti et al., 2020).

85 Knowledge of landslide hazard requires the assessment of “where” landslides might  
86 occur or re-activate, “when” or how frequently they can happen, and “how large” they  
87 will be (Guzzetti et al., 2005; Alvioli et al., 2018). The first task entails landslide  
88 susceptibility analyses, *i.e.*, the evaluation of landslide spatial occurrence. During past  
89 decades, a variety of landslide susceptibility analyses have been conducted at different  
90 scales with various mapping units, different geo-environmental conditions, and  
91 numerous methods and techniques (*e.g.*, Guzzetti et al., 2005; Van Den Eeckhaut et al.,  
92 2012; Alvioli et al., 2016; Stanley and Kirschbaum, 2017).

93 The aim of landslide susceptibility analyses is to assign different likelihoods for  
94 landslide occurrence, and classify different spatial locations in different susceptibility  
95 levels. Recently, some authors prepared systematic reviews on global and regional  
96 landslide susceptibility analyses, and highlighted their definitions, methods, model  
97 evaluations, achievements and limitations (*e.g.*, Budimir et al., 2015; Huang and Zhao,  
98 2018; Reichenbach et al., 2018). Practical uses of susceptibility analyses are often  
99 limited by large uncertainties and inconsistencies of various input data, and difficulties  
100 to understand the different susceptibility maps based on numerous methods  
101 (Reichenbach et al., 2018).

102 On the other hand, a few authors considered “non-susceptibility” analyses,  
103 consisting in identifying areas where the probability of landslide occurrence is  
104 negligible or null. Godt et al. (2012) first proposed a threshold-based method to define  
105 areas with negligible likelihood of landslide occurrence, further defined as non-  
106 susceptible areas by Marchesini et al. (2014). These statistically based non-  
107 susceptibility analyses establish a morphometric threshold by using geographically  
108 consistent data, and provide a simple and practical way to determine non-susceptible  
109 areas by using only morphometric information and accurate landslide data. Compared

110 with susceptibility analysis, non-susceptibility modeling reduced the uncertainties from  
111 input data and methods.

112 Non-susceptible areas are landslide-safe areas, which are the areas of choice for  
113 population and settlements in land management and planning, and for evacuation and  
114 resettlement in disaster responses. Overlaying non-susceptibility and population or  
115 settlement maps provides a way to illustrate the portion of population or settlements  
116 that are not exposed to landslide occurrence (Marchesini et al., 2014), and it provides  
117 strategies for decision-making in land planning and disaster mitigation. Moreover, Godt  
118 et al. (2012) highlighted a potential application of non-susceptibility maps as a proxy  
119 for landslide susceptibility analyses by relating the “not non-susceptible” class with  
120 “moderate” or “high” susceptibility classes. This work provides such a tool in the global  
121 scale, using data available in a homogeneous way.

122 Both Godt et al. (2012) and Marchesini et al. (2014) assumed terrain slope and relief  
123 as key variables for selecting landslide non-susceptible locations, at pixel level. The  
124 key assumption of non-susceptibility analyses is that flat, low-relief regions are not  
125 prone to landslides, which is supported by the fact that topography is the main  
126 influencing factor in landslide susceptibility analysis (Dai et al., 2002; Hong et al.,  
127 2007a; Stanley and Kirschbaum, 2017; Broeckx et al., 2018). Since the model is data-  
128 driven, a standard procedure for performance evaluation is required. Godt et al. (2012)  
129 established their model based on five state inventories with wide spatial and temporal  
130 coverage and landslide of all types, and tested their proposed non-susceptibility map by  
131 comparing with previous susceptibility analysis in the conterminous United States.  
132 Marchesini et al. (2014) conducted model fitting, testing and comparison by using  
133 different landslide inventories and different statistical methods. Their work revealed a  
134 low false positive rate (*FPR*) of about 0.06 for the quantile non-linear (QNL) non-

135 susceptibility model based on accurate and complete landslide inventories in Italy and  
136 Spain. The study obtained a well-validated non-susceptibility model.

137 Existing non-susceptibility analyses are focused on regional scales, *i.e.*, in the  
138 conterminous United States (Godt et al., 2012), Italy and Mediterranean region  
139 (Marchesini et al., 2014), whereas many authors have worked on global landslide  
140 susceptibility (*e.g.*, Nadim et al., 2006; Farahmand and Aghakouchak, 2013; Stanley  
141 and Kirschbaum, 2017). In their review of landslide susceptibility models, Reichenbach  
142 et al. (2018) recommended extending and further testing the “non-susceptible” terrain  
143 zonation in different geographical regions as to validate its applicability and serve as a  
144 proxy for global or regional landslide susceptibility and hazard assessment.

145 In this study, we first tested and validated the QNL model proposed by Marchesini  
146 et al. (2014) based on available global and regional landslide datasets. We used two  
147 global datasets, seven national datasets and nine regional datasets, and obtained relief  
148 and slope data from the ~90-m Shuttle Radar Topography Mission (SRTM) digital  
149 elevation model (DEM). We proposed a global landslide non-susceptibility map  
150 (GLNSM) based on the existing QNL model by Marchesini et al. (2014), and compared  
151 the proposed non-susceptibility map with existing global or continental susceptibility  
152 and non-susceptibility maps. Eventually, we estimated the global population size and  
153 settlement area not exposed to landslides as a potential application of this work. For  
154 further extending analyses of non-susceptibility, we investigated new QNL models for  
155 several regions and global models based on different landslide types.

## 156 **2. Data**

### 157 **2.1 Topography data**

158 The SRTM DEM is a quasi-global terrain elevation dataset, available between 60°N  
159 and 60°S latitude, and widely used in topographical information extraction. First

160 released in 2003, version 4.1 is now available (<https://srtm.csi.cgiar.org/srtmdata/>;  
161 accessed on 18 December 2020; Jarvis et al., 2008). Existing non-susceptibility  
162 analyses were conducted based on SRTM DEM ~90-m data of version 2 (Marchesini  
163 et al., 2014), which is a “finished” product covering the global landmasses, but contains  
164 regions with missing data (Jarvis et al., 2008). The spatial accuracy of topographical  
165 information is of great importance for non-susceptibility analysis. In the new version  
166 of dataset, void pixels were filled with available high-resolution auxiliary regional  
167 DEMs and a series of interpolation techniques (Reuter et al., 2007).

168 In this study, we used DEM data of the latest version, with ~90-m resolution at the  
169 equator, in the original geographical (longitude and latitude) coordinate reference  
170 system (CRS, in WGS84, EPSG: 4326). Elevation data was used to calculate regional  
171 relative relief ( $R$ ) and local terrain slope ( $S$ ), the two morphometric variables used in  
172 the non-susceptibility model.

## 173 **2.2 Landslide datasets**

174 Landslide data is vital for calibrating and validating susceptibility and non-  
175 susceptibility maps. Despite widely present around the world, reported and mapped  
176 landslides are available only in part of the landmasses. Detailed information with high  
177 accuracy and completeness is lacking (Guzzetti et al., 2012). The USA National  
178 Aeronautics and Space Administration (NASA) landslide team launched the Global  
179 Landslide Catalog (GLC), in which records are available with occurrence dates and  
180 locations, types, triggers and estimates of location accuracy since 2007 (Kirschbaum et  
181 al., 2010, 2015). To improve the completeness of landslide dataset, NASA subsequently  
182 launched the Cooperative Open Online Landslide Repository (COOLR; Juang et al.,  
183 2019), which is a product of citizen science and original researches, containing  
184 landslide points and related alphanumeric records updated until August, 2020

185 (<https://gpm.nasa.gov/landslides/>; accessed on 18 December 2020). To ensure the  
186 accuracy of the dataset, they added a measurement of location accuracy for each  
187 landslide event based on multiple sources. The Global Fatal Landslide Database (GFLD)  
188 is another global landslide dataset, listing landslides that caused deaths from 2004 to  
189 2017, and including landslides triggered by different non-seismic causes, *e.g.*, rainfall  
190 and human activities (Froude and Petley, 2018; Petley and Froude, 2019). The location  
191 accuracy in GFLD is estimated based on geographical units such as villages or states.

192 Regional landslide datasets are also available for some specific nations and areas.  
193 These datasets were compiled by detailed image interpretation (*e.g.*, McKeon, 2016),  
194 disaster reports (*e.g.*, YNDPMC, 2016), newsfeeds (*e.g.*, Li et al., 2016), and partly  
195 aided by field surveys. In USA, the U.S. Geological Survey leads the landslide  
196 monitoring (USGS, 2020). Statewise landslide inventories are available in Arizona  
197 (Cook et al., 2016), Oregon (Burns and Madin, 2009), Utah (Elliott and Harty, 2010),  
198 Vermont (Cliff and Springston, 2012) and Washington (Slaughter et al., 2017).  
199 Systematic information for landslide occurrence is obtained from geologic maps, aerial  
200 photo and imagery interpretation, and GIS/GPS tools. Some of records are even  
201 checked in field, whereas some are just searched and digitized via news and report  
202 sources. In Europe, there is pan-European cooperation in landslide hazard and risk  
203 assessment (Wilde et al., 2018), and landslide inventories are conducted in most of the  
204 countries (Van Den Eeckhaut and Hervás, 2012). However, the datasets are not publicly  
205 available. In Italy, inventory FraneItalia includes events occurring between 2010 and  
206 2019 (v2.0; Calvello and Pecoraro, 2018). This catalog is an interpretation product of  
207 news, reports and other text-based sources, presenting the location accuracy with three  
208 confidence descriptors named as certain, approximated and municipality (available:  
209 <https://data.mendeley.com/datasets/compare/zygb8jygrw/1/2>; accessed on 18

210 December 2020). Ireland has a long history of landslide inventory development  
211 (Creighton, 2006). The latest version of Ireland national landslide dataset was derived  
212 from high-resolution aerial photo interpretation spanning from 2000 to 2010, with  
213 validation in field and a 3D visualisation system (McKeon, 2016). In Oceania, spatial  
214 information of the inventoried landslides was developed in Australia (Osuchowski and  
215 Atkinson, 2008) and New Zealand (Rosser et al., 2017). The Australian landslide  
216 database was recently updated in 2018, and firstly launched under collaborative efforts  
217 of the federal, state and local. A statewise inventory was also developed in Tasmania  
218 (Mazengarb and Stevenson, 2010). The majority of the information was sourced from  
219 national and state reports, news and other publications, and adjusted more accurately  
220 based on aerial photograph interpretation and mapping. The New Zealand landslide  
221 database (NZLD) is a combined inventory to hold a number of existing landslide  
222 datasets (Rosser et al., 2017). Some of the data sources were derived from aerial photo  
223 interpretation with high-quality control. However, the public dataset is shared with no  
224 accuracy information. In China, a comprehensive national landslide dataset was  
225 published based on official documents, news reports and existing web databases (Li et  
226 al., 2016). The measurement of location accuracy is lacking. In two provinces of China,  
227 Guangdong and Yunnan, landslide information of about twenty years is available in the  
228 printed yearbook of disaster prevention and mitigation (GDDPMC, 2016; YNDPMC,  
229 2016). The uncertainty of the position can be measured with two descriptors:  
230 approximated (village or street) and municipality (town). In Turkey, a fatal landslide  
231 dataset was recently produced and the uncertainty of the location varies from  
232 district/village to city (Görüm and Fidan, 2021).

233       Uncertainties exist for landslide datasets, especially the occurrence location. One  
234 reason is resulted from accidental error from data sources and systematic error from

235 geographical transformation (Guzzetti et al., 2012; Froude and Petley, 2018). Moreover,  
236 the typical characteristics for certain landslide types makes it not easy to accurately  
237 locate their location such as rapid landslides, which may occur quickly and travel in a  
238 long way. To ensure the accuracy of landslide data, preliminary analysis and selection  
239 were conducted. For example, data entries with location accuracy less than 1 km were  
240 chose in COOLR and GFLD dataset. For regional databases with detailed data sources,  
241 records derived from imagery interpretation, GIS methods or field check were used,  
242 such as Australian, Oregon and Tasmanian datasets; for other datasets, landslide events  
243 were selected based on given position descriptors, such as Italian, Turkish, Guangdong  
244 and Yunnan datasets (the “certain” and “approximated” records were used). For NZLD,  
245 we selected landslides with detailed occurrence time, and discarded these with no  
246 occurrence time. Specifically, all the data entries were used for the Chinese datasets.  
247 Some of datasets (e.g., Ireland and Oregon datasets) are provided with both point and  
248 polygon landslide features, of which recorded landslide events are not exactly the same  
249 owing to the different data sources or mapping methods. Thus, both of them are used  
250 in our validation. All the datasets were projected in the WGS84 CRS (EPSG: 4326).  
251 Table 1 lists summary information of the landslide data used in this work, including  
252 two global datasets, seven national datasets and nine regional datasets, six of which  
253 include landslides mapped as polygons. Detailed location accuracy, landslide type and  
254 trigger information for each dataset are available in a supplement excel file. Figure 1  
255 shows the administrative geographic extent of national and regional datasets (a global  
256 view and four regional views).

257 Insert Table 1

258 Insert Fig. 1

### 259 **2.3 Landslide susceptibility and non-susceptibility maps**

260 Whereas non-susceptibility represents zero or negligible likelihood of landslide  
261 occurrence, susceptibility classes represent well-defined intervals of likelihood of  
262 landslide occurrence in conventional susceptibility maps. To show a link between the  
263 two types of analyses, we compared non-susceptibility in GLNSM with the lowest  
264 susceptibility class in existing global and continental susceptibility maps. During the  
265 two past decades, large-scale susceptibility analyses have been widely prepared in  
266 Europe, Africa, and the world. Early global susceptibility maps were proposed by  
267 Nadim et al. (2006) and Hong et al. (2007a). In this study, we used three updated global  
268 susceptibility/risk maps proposed by Giuliani and Peduzzi (2011), Stanley and  
269 Kirschbaum (2017) and Lin et al. (2017), and two continental maps published by  
270 Broeckx et al. (2018) and Wilde et al. (2018) for Africa and Europe, respectively. All  
271 the above susceptibility maps show five classes (very low, low, moderate, high, and  
272 very high susceptibility), although the methods and criteria to define them are different  
273 across different studies.

274 In the conterminous United States, Godt et al. (2012) proposed a national landslide  
275 non-susceptibility map based on a general linear model (GLM;  $S_{90} = 0.19R_{90} -$   
276  $0.16, 6^\circ \leq S_{90} \leq 21^\circ$ ), in which  $R_{90}$  and  $S_{90}$  represent the 90<sup>th</sup> percentiles of relief and  
277 slope values in each given landslide feature or pixel cell, respectively. Here we  
278 reconstructed the map based on the GLM model with slope and relief data prepared in  
279 our work to conduct a regional comparison with our global non-susceptibility map.

## 280 **3 Methods**

### 281 **3.1 Non-susceptibility model**

282 The existing non-susceptibility model proposed by Marchesini et al. (2014) provided a  
283 minimum threshold curve of relief v.s. slope corresponding to historical landslide  
284 events. Below the threshold, landslide susceptibility is expected to be null or negligible,

285 and thus non-susceptible areas are singled out. The QNL model performed best among  
286 all of the models considered by Marchesini et al. (2014) in terms of *FPR*. The analysis  
287 considered Italian regional and high-quality landslide inventories, which were compiled  
288 through image interpretation and field campaigns between 1993 and 2013. The  
289 inventories contain almost all landslide types, and the majority of the landslides are  
290 rotational and translational slides, earth flows, complex, and compound movements  
291 according to the Cruden and Varnes (1996) classification schemes. The inventories  
292 cover most landslide-prone physiographical regions in Italy, which differ in lithological,  
293 climatic and land cover conditions (Guzzetti et al., 2012; Peruccacci et al., 2017; Alvioli  
294 et al., 2020). The QNL model was validated with an Italian national landslide inventory  
295 (Trigila et al., 2010), and a Spanish inventory. The QNL model is:

$$296 \quad S = \alpha e^{\beta R}, \quad (1)$$

297 where  $S$  is the local terrain slope in degrees;  $R$  is the regional relative relief in meters,  
298 ranging between 0 and 1,000 m;  $\alpha=3.539$  and  $\beta=0.0028$  are regression parameters.  
299 Equation (1) represents the model's threshold: pixels whose representative point on the  
300  $(R, S)$  plane falls below the curve are non-susceptible to landslide occurrence with 5%  
301 expected misclassifications. Validation of the model by Marchesini et al. (2014)  
302 revealed a *FPR* of 0.06, ranging from 0.05 for translation and rotational slide to 0.21  
303 for lateral spread.

304 In this work, we tested the applicability of the data-driven QNL model proposed by  
305 Marchesini et al. (2014) for a worldwide application. The extrapolation of the model,  
306 from regional to global scale, indicates a large range of relief values (more than 1,000  
307 m), which was the validity range of the QNL model of Marchesini et al. (2014). Thus,  
308 we applied a maximum slope threshold of  $58^\circ$  (corresponding to the case when relief  
309 in the  $15 \times 15$  window is equal to 1,000 m in Eq. 1), assuming areas with slope values

310 over 58° as highly landslide-prone (Nadim et al., 2006; Hong et al., 2007a). A  
 311 maximum slope threshold was also used in Godt et al. (2012). Moreover, we tried to  
 312 propose new non-susceptibility models based on available landslide data for different  
 313 regions and landslide types, to show their effects on non-susceptibility zonation.

### 314 **3.2 Regional relative relief and local terrain slope calculation**

315 Regional relative relief and local terrain slope are two basic inputs in landslide  
 316 susceptibility and non-susceptibility analysis, and other branches of earth sciences.  
 317 Marchesini et al. (2014) calculated  $S$  by elevation gradient within a 3×3-pixel moving  
 318 window, and extracted  $R$ , the difference between maximum and minimum elevation,  
 319 within a 15×15-pixel moving window. The aim of selecting different moving windows  
 320 for two variables is to reduce their collinearity and capture the significantly different  
 321 morphometric characteristics related to landscape evolution.

322 Pixel size difference at different latitudes was taken into account, for the calculation  
 323 of slope, as follows. Firstly, the widths of each pixel cell in the longitude ( $\delta x_{i,j}$ ) and  
 324 latitude ( $\delta y_{i,j}$ ) direction were calculated based on the geometry of the earth WGS84  
 325 ellipsoid; then the slope components in the longitude and latitude direction were defined  
 326 by the partial derivatives of the polynomial to use most of elevation ( $z_{i,j}$ ) information  
 327 in a moving window, which are defined as follows:

$$328 \quad \frac{\delta z_{i,j}}{\delta x_{i,j}} = \frac{(z_{i+1,j+1} + 2z_{i+1,j} + z_{i+1,j-1}) - (z_{i-1,j+1} + 2z_{i-1,j} + z_{i-1,j-1})}{8\delta x_{i,j}}, \quad (2)$$

$$329 \quad \frac{\delta z_{i,j}}{\delta y_{i,j}} = \frac{(z_{i+1,j+1} + 2z_{i,j+1} + z_{i-1,j+1}) - (z_{i+1,j-1} + 2z_{i,j-1} + z_{i-1,j-1})}{8\delta y_{i,j}}, \quad (3)$$

330 Finally, the slope ( $S_{i,j}$ ) in degree was obtained from its components in two direction.

331 
$$S_{i,j}$$

332 
$$= \arctan \left( \left( \frac{\delta z_{i,j}}{\delta x_{i,j}} \right)^2 + \left( \frac{\delta z_{i,j}}{\delta y_{i,j}} \right)^2 \right)^{1/2}, \quad (4) \text{Figure}$$

333 
$$\text{Insert Fig. 2}$$

### 334 **3.3 Validation procedure**

335 The proposed GLNSM map was validated with independent landslide datasets (in  
 336 Section 2.2). For datasets containing polygon features, we overlaid the vector maps  
 337 with the global relief and slope maps, and extracted the 90<sup>th</sup> quantile (Godt et al., 2012)  
 338 of relief and slope values in each polygon. We assumed the 90<sup>th</sup> quantile of  $S$  and  $R$   
 339 values as corresponding to the landslide-triggering portion of the landslide body (Godt  
 340 et al., 2012).

341 For each landslide dataset, we calculated the  $FPR = FP / (FP + TN)$ , where  $FP$  is  
 342 the number of false positives, i.e., landslides below the  $R$ - $S$  threshold of Eq. (1), and  
 343  $TN$  is the number of true negatives, i.e., landslides above the  $R$ - $S$  threshold.

344 To consider the inherent uncertainties associated with the landslide locations in  
 345 point datasets, we considered a circular 1-km buffer for each landslide point, and then  
 346 conducted the same evaluation of  $FPR$  used for the polygon datasets. We further  
 347 considered reactivations within a 1-km buffer as a single record in the landslide datasets,  
 348 to avoid artificially increasing the values of  $FP$  or  $TN$  (Biasutti et al., 2016; Benz and  
 349 Blum, 2019).

## 350 **4. Results and discussions**

### 351 **4.1 Non-susceptibility model: validation against landslide datasets**

352 For each landslide dataset (Table 1), we extracted morphological characteristics based  
 353 on location information of landslides and plotted their relief and slope (Fig. 3). Based  
 354 on the QNL non-susceptibility model,  $FPR$  was calculated. Thirteen out of eighteen

355 datasets have  $FPR < 0.15$ , and five have less than 10% of landslides located in non-  
356 susceptible areas ( $FPR < 0.10$ ). Overall, we grouped the eighteen datasets into a single  
357 one, including all of the records. It turns out that about 12% of the landslides are located  
358 in non-susceptible areas (Table 2; in total, 39,608 individual landslides were  
359 considered). The percentage is lower for translational/rotational slides, earth flows  
360 ( $FPR = 0.09$ ), and flows (0.05). The results coincide with the good performances of  
361 QNL non-susceptibility model for translational/rotational slide and slow flow in  
362 Marchesini et al. (2014). By comparison, performance is poor for debris flows,  
363 mudslides and earth slides. Performance associated to rapid landslides is poor in  
364 Marchesini et al. (2014) as well. The reason may lie in the typical low slope associated  
365 to mudslides, and rapid development of debris flows, which can also travel into nearly  
366 flat areas (travel angle values can be also equal to  $4^\circ$ , Rickenmann, 2005). Moreover,  
367 rapid landslides are always triggered by heavy rain or huge fluctuations of earth owing  
368 to instantaneous strength loss (such as liquefaction of granular soils; Hungr, 2007).  
369 Thus, they could occur at lower slopes.

370 Insert Fig. 3

371 Insert Table 2

372 For global datasets, COOLR has a better match with the QNL model than GFLD.  
373 Figure 3a and b, respectively, show a direct comparison on the  $(R, S)$  plane of COOLR  
374 and GFLD datasets with the threshold of Eq. (1). In this case, the reason may lie in the  
375 fact that GFLD is a dataset containing only fatal landslides with lower overall  
376 representativeness and, most importantly, with a relative abundance of rapid landslides  
377 that typically cause more deaths due to their runouts extending on the flat areas.

378 In the case of regional datasets, Ireland, New Zealand, Oregon and Tasmania (Fig.  
379 3e, i, l and n) have good performance,  $FPR < 0.05$ , while Australia and China (Fig. 3c

380 and d) have poor performance,  $FPR \geq 0.20$ . We maintain that the non-susceptibility  
381 model works well with an overall low  $FPR$  and good performance.

382 Marchesini et al. (2014) highlighted the importance of accurate and complete  
383 landslide information for the non-susceptibility zonation. Here, we used the density of  
384 landslide events ( $N_L$ : number of landslide records per  $10^3 \text{ km}^2$  for each dataset, in  
385 Table 1), as a proxy of completeness, exploring the relationship between  $N_L$  and  $FPR$ .

386 Global datasets are excluded from this analysis, due to their manifest poor  
387 completeness. Figure 4 indicates that a linear relationship exists between  $FPR$  and  $N_L$ .  
388 As  $N_L$  increases,  $FPR$  decreases, suggesting that high landslide density might improve  
389 the performance of validation. The reason of high  $FPR$ s in Australia, China and  
390 Arizona (Fig. 3c, d and j) probably lie in the poor completeness of landslide datasets.

391 Further application of non-susceptible analyses requires more complete landslide  
392 datasets, and the number of reported landslides per area of Vermont ( $0.014 \text{ km}^{-2}$ )  
393 could be a reference to assess the completeness of landslide inventories with an  
394 expected good  $FPR$  (less than 0.10 for point datasets and 0.15 for polygon datasets)

395 based this linear relationship. Insert Fig. 4

## 396 **4.2 Global landslide non-susceptibility map**

397 An overall good performance is illustrated for QNL model proposed by Marchesini et  
398 al. (2014) for available global and regional datasets in Section 4.1. Thus, we proposed  
399 a global landslide non-susceptibility map to show the distribution of landslide non-  
400 susceptible areas in  $\sim 90\text{-m}$  resolution (Fig. 5). The map indicates that 82.9% of global  
401 landmasses are located in non-susceptible areas, higher than the percentage of non-  
402 mountainous areas (69.5%; Sayre et al., 2018), suggesting that some of the mountainous  
403 areas are relatively stable. A further overlaying analysis reveals that GLNSM  
404 encompasses 80% of the global non-mountainous areas. Marchesini et al. (2014) quoted

405 63% for the percentage of non-susceptible areas in the Mediterranean region, which is  
406 expected, given that Mediterranean region is highly prone to landslide occurrence  
407 (Wilde et al., 2018). The corresponding percentages of non-susceptible areas are also  
408 low in Asia (74.8%) and North America (78.5%; Fig. 5a), corresponding to high fatal  
409 landslide incidence in the Western North America, and Southern, Eastern and  
410 Southeastern Asia (Froude and Petley, 2018). Regional views (Fig. 5 b-e) show low  
411 percentages of non-susceptible areas in the western United States, Italy, the eastern  
412 Australia, New Zealand, and the Himalayas, in agreement with landslide hotspots in  
413 previous studies (Kirschbaum et al., 2015; Haque et al., 2019).

414 Insert Fig. 5

415 As stated in Godt et al. (2012), landslide susceptibility maps are possible choice for  
416 testing the applicability of GLNSM. For available global and continental susceptibility  
417 maps in Section 2.3, the very-low class of each map was overlaid with our non-  
418 susceptibility map. The comparison revealed that worldwide 91.5% of the “very low”  
419 susceptibility pixels are located in non-susceptible areas, and specifically in the  
420 European susceptibility map and the global map proposed by Stanley and Kirschbaum  
421 (2017), more than 99% of the pixels classified with the very-low susceptibility are  
422 located in non-susceptible areas (Table 3).

423 Insert Table 3

424 We further compared the GLNSM with the national non-susceptibility map in the  
425 conterminous United States. Figure 6 shows the two non-susceptibility maps in the  
426 region, based on the GLM and QNL models. The two maps share similar spatial  
427 distribution of non-susceptible areas. They almost hold the same pattern in the western  
428 and eastern USA, where high incidence of landslides exists. The two maps coincide  
429 with each other in about 80% of the area of the conterminous USA, while the map of

430 GLM model (Fig. 6b) predicts less non-susceptible areas in the western and middle  
431 USA than that of QNL model, and the reverse in the eastern USA. The GLM model  
432 was established in a narrow interval, *i.e.*, [6°, 21°], of local terrain slope and not  
433 validated with any landslide dataset. Actually, the slope values range from 0° to 71° in  
434 the conterminous USA (Fig. 2), and only about 25% of the landmasses has a local  
435 terrain slope in the interval of [6°, 21°]. Thus, large portion of the landmasses remains  
436 undefined within the GLM model. The above consideration partly explains the  
437 discrepancies between the two maps. Region QNL model based on available USA state  
438 datasets reveals a lower *R-S* threshold compared with the QNL model by Marchesini et  
439 al. (2014) (see Section 4.4). Thus, further investigations are needed to conduct regional  
440 non-susceptibility analyses with more accurate and complete landslide inventories.

441 Insert Fig. 6

#### 442 **4.3 Relevance of the non-susceptibility map**

443 Marchesini et al. (2014) conducted a non-exposure analysis to estimate sizes of  
444 settlement and population to possible landslide occurrence. The non-exposure outputs  
445 are relevant for decision-making in disaster prevention, land management and planning.

446 We conducted non-exposure analysis by using grid settlement data in 2014 and  
447 population data in 2015 with ~1-km resolution, available from the Global Human  
448 Settlement Layer Data Package (Florczyk et al. 2019). The human settlement data is a  
449 product derived from the Global Land Survey Landsat image, and the population data  
450 were disaggregated and resampled from the Gridded Population of the World  
451 provided by the Center for International Earth Science Information Network of  
452 Columbia University. Global overlay of these layers with the GLNSM reveals that  
453 91.2% of built-up areas, and 91.8% of the population are located in non-susceptible  
454 areas (Table 4), more than the percentage of non-susceptible areas itself (82.9%;

455 Table 2). The majority of people and buildings are located in relatively safe  
456 conditions, and the density of built-up area and population size in non-susceptible  
457 areas is greatly larger (over two times) than that in “not non-susceptible” areas. Insert

458 Table 4

#### 459 **4.4 Regional and landslide type effects on non-susceptibility analysis**

460 Whereas geological environments may influence the spatial pattern of landslide  
461 occurrence and failure mechanisms vary with landslide types (e.g., Jia et al., 2020), we  
462 try to establish QNL non-susceptibility models for different regions and landslide types  
463 as compared with the model proposed by Marchesini et al. (2014). We grouped the  
464 landslide datasets as four new datasets based on regional views in Figure 1, and labeled  
465 as Region B (Fig. 1b), C (Fig. 1c), D (Fig. 1d) and E (Fig. 1e), respectively. A global  
466 model was also established based on the COOLR dataset. To establish models of  
467 different landslide types, we only considered the COOLR dataset to assure consistent  
468 landslide information. Here, debris flows, translational/rotational slides, mudslides,  
469 rock falls, complex landslides and others are considered.

470 Relief-slope thresholds in the globe and four regions (Fig. 7), for six landslide types  
471 (Fig. 8) are lower than the QNL model proposed by Marchesini et al. (2014) (denoted  
472 by Model\_Ma). The minimum slope threshold values ( $\alpha$ ) for regions vary from about  
473 1.2 to 3.7 (Table 5), less than that of Model\_Ma except for Region E. The threshold  
474 curve of Region E (Fig. 7e; based on Australia, New Zealand and Tasmania datasets)  
475 is the closest to Model\_Ma. Region C (Fig. 7c; based on China, Guangdong and Yunnan  
476 datasets) and D (Fig. 7d; based on Ireland, Italy and Turkey datasets) share the same  
477 scale value ( $\beta$ ). There are big differences between the models of Region B (Fig. 7b;  
478 based on USA state datasets) and other models. Significant differences exist among  
479 models of different types. The curve of complex landslides (Fig. 8e) is most similar to

480 Model\_Ma, while debris flows and mudslides give rise to lower minimum slope  
481 thresholds (Table 5). We concluded that the influence of geological and type factors  
482 cannot be ignored for further extending analyses of non-susceptibility, though the non-  
483 susceptibility models for different regions and landslide types in this study are not  
484 enough to conduct regional or global non-susceptibility analyses.

485 Insert Fig. 7

486 Insert Fig. 8

487 Insert Table 5

## 488 **5. Conclusions**

489 This study aimed at preparing a global landslide non-susceptibility map to highlight the  
490 areas where expected landslide susceptibility is null or negligible, by extending the  
491 model trained in Italy and applied to the Mediterranean region by Marchesini et al.  
492 (2014), with a maximum slope threshold of  $58^\circ$ . Non-susceptible areas were singled  
493 out by means of a relief-slope QNL threshold, with expected 5% misclassifications.  
494 Our findings are as follows:

495 1) The GLNSM (Fig. 5) obtained here covers 82.9% of global landmasses.

496 2) The QNL model proposed by Marchesini et al. (2014) shows good classification  
497 performance against global and regional datasets, with overall  $FPR = 0.12$  (Table 2).  
498 Some regional landslide datasets (Fig. 3) and datasets grouped by landslide types (Table  
499 2) score with lower  $FPR$  (better performances) with respect to the global result. We  
500 maintain that the non-susceptibility model works well when uncertainty on landslide  
501 location is reduced.

502 3) The GLNSM is generally consistent with the “very-low” susceptibility class in  
503 existing global and continental susceptibility maps (Table 3), and shares a similar  
504 spatial distribution with the national non-susceptibility map in USA (Fig. 6).

505 4) The GLNSM is promising for decision-making in land planning and disaster  
506 responses. Globally, 91.8% of the population lives, and 91.2% of the settlements are  
507 located, in non-susceptible areas (Table 4). The population and built-up densities are  
508 significantly higher in non-susceptible areas compared with that outside the non-  
509 susceptible areas.

510 5) Non-susceptibility analyses are significantly influenced by landslide types (Fig.  
511 8). Moreover, quantile models obtained in different regions (Fig. 7) are significantly  
512 different. This suggests that considering the variability of geological setting, and  
513 landslide type, is mandatory for further extending regional non-susceptibility analyses.

514 The GLNSM proposed in this work, or analogous local maps derived from higher-  
515 resolution DEMs, can be a useful tool to illustrate where the likelihood of landslide  
516 occurrence is zero or negligible. We suggest that the map can be used for a priori  
517 exclusion of non-susceptible areas from susceptibility zonation (Alvioli et al., 2016).  
518 Moreover, for landslide early warning systems, an easy-to-interpret map of areas with  
519 zero likelihood of landslide occurrence could simplify decision making, to focus on  
520 areas outside the non-susceptible area. Indeed, the map of Marchesini et al. (2014)  
521 served to that purpose for national landslide warning system in Italy (Guzzetti et al.,  
522 2020). We maintain that our global map might be useful for a global knowledge of  
523 landslide hazard and risk assessment.

## 524 **References**

525 AGS, 2015. Natural Hazards in Arizona. Arizona Geological. Survey. Available:  
526 [https://uagis.maps.arcgis.com/apps/webappviewer/index.html?id=98729f76e464](https://uagis.maps.arcgis.com/apps/webappviewer/index.html?id=98729f76e4644f1093d1c2cd6dabb584)  
527 [4f1093d1c2cd6dabb584](https://uagis.maps.arcgis.com/apps/webappviewer/index.html?id=98729f76e4644f1093d1c2cd6dabb584) (accessed 18 December 2020).  
528 Alvioli, M., Guzzetti, F., Marchesini, I., 2020. Parameter-free delineation of slope units  
529 and terrain subdivision of Italy. *Geomorphology* 358.

530 <https://doi.org/10.1016/j.geomorph.2020.107124>.

531 Alvioli, M., Marchesini, I., Reichenbach, P., Rossi, M., Ardizzone, F., Fiorucci, F.,  
532 Guzzetti, F., 2016. Automatic delineation of geomorphological slope units with  
533 r.slopeunits v1.0 and their optimization for landslide susceptibility modeling.  
534 *Geosci. Model Dev.* 9, 3975–3991. <https://doi.org/10.5194/gmd-9-3975-2016>.

535 Alvioli, M., Melillo, M., Guzzetti, F., Rossi, M., Palazzi, E., von Hardenberg, J.,  
536 Brunetti, M. T., Peruccacci, S. (2018). Implications of climate change on landslide  
537 hazard in central Italy. *Science of the Total Environment* 630, 1528-1543.  
538 <https://doi.org/10.1016/j.scitotenv.2018.02.315>.

539 Benz, S.A., Blum, P., 2019. Global detection of rainfall-triggered landslide clusters.  
540 *Nat. Hazards Earth Syst. Sci.* 19, 1433–1444. [https://doi.org/10.5194/nhess-19-](https://doi.org/10.5194/nhess-19-1433-2019)  
541 [1433-2019](https://doi.org/10.5194/nhess-19-1433-2019).

542 Biasutti, M., Seager, R., Kirschbaum, D.B., 2016. Landslides in West Coast  
543 metropolitan areas: The role of extreme weather events. *Weather Clim. Extrem.*  
544 14, 67–79. <https://doi.org/10.1016/j.wace.2016.11.004>.

545 Budimir, M.E.A., Atkinson, P.M., Lewis, H.G., 2015. A systematic review of landslide  
546 probability mapping using logistic regression. *Landslides* 12, 419–436.  
547 <https://doi.org/10.1007/s10346-014-0550-5>.

548 Broeckx, J., Vanmaercke, M., Duchateau, R., Poesen, J., 2018. A data-based landslide  
549 susceptibility map of Africa. *Earth-Science Rev.* 185, 102–121.  
550 <https://doi.org/10.1016/j.earscirev.2018.05.002>.

551 Burns, W.J., Madin, I.P., 2009. Protocol for inventory mapping of landslide deposits  
552 from light detection and ranging (lidar) imagery. Oregon Department of Geology  
553 and Mineral Industries, Special Paper 42.  
554 <https://digital.osl.state.or.us/islandora/object/osl%3A24647/datastream/OBJ/dow>

555 nload/Protocol\_for\_inventory\_mapping\_of\_landslide\_deposits\_from\_light\_detec  
556 tion\_and\_ranging\_lidar\_imagery.pdf.

557 Calvello, M., Pecoraro, G., 2018. FraneItalia: a catalog of recent Italian landslides.  
558 Geoenvironmental Disasters 5, 13. <https://doi.org/10.1186/s40677-018-0105-5>.

559 Cliff, A.E., Springston, G, 2012. Protocol for identification of areas sensitive to  
560 landslide hazards in Vermont. Vermont Geological Survey, Technical report.  
561 [https://dec.vermont.gov/sites/dec/files/geo/TechReports/VGTR2012-  
562 1LandslideProtocol.pdf](https://dec.vermont.gov/sites/dec/files/geo/TechReports/VGTR2012-1LandslideProtocol.pdf).

563 Cook, J.P., Pearthree, P.A., Gootee, B.F., Conway, B.D., Youberg, A., 2016.  
564 Landslides are surprisingly large and widespread in Arizona. Geological Society  
565 of America Annual Conference, Colorado, United States.  
566 <https://repository.arizona.edu/handle/10150/629611>. Creighton, R., 2006.  
567 Landslides in Ireland: A report of the Irish landslides working group. Geological  
568 Survey of Ireland, Technical report.  
569 [https://www.gsi.ie/documents/Landslides\\_in\\_Ireland\\_2006.pdf](https://www.gsi.ie/documents/Landslides_in_Ireland_2006.pdf).

570 Cruden, D.M., Varnes, D.J., 1996. Landslide types and processes, in: Turner, A.K.,  
571 Schuster, R.L. (Eds.), Landslides: Investigation and mitigation. National Academy  
572 Press, Washington DC, USA, pp. 1–77.

573 Dai, F.C., Lee, C.F., Ngai, Y.Y., 2002. Landslide risk assessment and management: An  
574 overview. Eng. Geol. 64, 65–87. [https://doi.org/10.1016/S0013-7952\(01\)00093-X](https://doi.org/10.1016/S0013-7952(01)00093-X)

575 Elliott, A.H., Harty, K.M., 2010. Landslide maps of Utah. Utah Geological Survey,  
576 Technical report.  
577 [https://www.utahmapstore.com/collections/landslides/products/m-  
578 246?variant=32205592592437](https://www.utahmapstore.com/collections/landslides/products/m-246?variant=32205592592437).

579 Farahmand, A., Aghakouchak, A., 2013. A satellite-based global landslide model. Nat.

580 Hazards Earth Syst. Sci. 13, 1259–1267. <https://doi.org/10.5194/nhess-13-1259->  
581 2013.

582 Florczyk, A.J., Corbane, C., Ehrlich, D., Freire, S., Kemper, T., Maffenini, L.,  
583 Melchiorri, M., Pesaresi, M., Politis, P., Schiavina, M., Sabo, F., Zanchetta, L.,  
584 2019. GHSL Data Package 2019. Luxembourg. <https://doi.org/10.2760/062975>.

585 Froude, M.J., Petley, D.N., 2018. Global fatal landslide occurrence from 2004 to 2016.  
586 Nat. Hazards Earth Syst. Sci. 18, 2161–2181. <https://doi.org/10.5194/nhess-18->  
587 2161-2018.

588 Gariano, S.L., Guzzetti, F., 2016. Landslides in a changing climate. Earth Sci. Rev. 162,  
589 227–252. <https://doi.org/10.1016/j.earscirev.2016.08.011>.

590 GDDPMC, 2016. Yearbook of disaster prevention and mitigation in Guangdong, China.  
591 Guangdong Disaster Prevention and Mitigation Committee, Technical report.  
592 [http://ss.zhizhen.com/detail\\_38502727e7500f262814f69715a39ba4e301f9b9028](http://ss.zhizhen.com/detail_38502727e7500f262814f69715a39ba4e301f9b9028)  
593 [d38f41921b0a3ea25510134114c969f2eae5c12132a9ac61ae8899d230af272b6db](http://ss.zhizhen.com/detail_38502727e7500f262814f69715a39ba4e301f9b9028)  
594 [831e76ddfdf533af545b1b44a1a422ad3ad80a977f299f2a8c?&apistrclassfy=0\\_21](http://ss.zhizhen.com/detail_38502727e7500f262814f69715a39ba4e301f9b9028)  
595 [\\_8](http://ss.zhizhen.com/detail_38502727e7500f262814f69715a39ba4e301f9b9028).

596 Geoscience Australia, 2012. Landslide Search. Canberra. Available:  
597 <http://pid.geoscience.gov.au/dataset/ga/74273> (accessed 18 December 2020).

598 Giuliani, G., Peduzzi, P., 2011. The PREVIEW global risk data platform: A geoportal  
599 to serve and share global data on risk to natural hazards. Nat. Hazards Earth Syst.  
600 Sci. 11, 53–66. <https://doi.org/10.5194/nhess-11-53-2011>.

601 Godt, J.W., Coe, J.A., Baum, R.L., Highland, L.M., Keaton, J.R., Roth, R.J., 2012.  
602 Prototype landslide hazard map of the conterminous United States, in: Eberhardt,  
603 E., Froese, C., Leroueil, S., Turner, K., (Eds.), Landslides and engineered slopes:  
604 Protecting society through improved understanding. Taylor & Francis Group,

605 London, pp. 245–250.

606 Görüm, T., Fidan, S., 2021. Spatiotemporal variations of fatal landslides in Turkey  
607 (online). *Landslides*. <https://doi.org/10.1007/s10346-020-01580-7>.

608 Guzzetti, F., Gariano, S.L., Peruccacci, S., Brunetti, M.T., Marchesini, I., Rossi, M.,  
609 Melillo, M., 2020. Geographical landslide early warning systems. *Earth-Science*  
610 *Rev.* 200, 102973. <https://doi.org/10.1016/j.earscirev.2019.102973>.

611 Guzzetti, F., Mondini, A.C., Cardinali, M., Fiorucci, F., Santangelo, M., Chang, K.T.,  
612 2012. Landslide inventory maps: New tools for an old problem. *Earth-Science Rev.*  
613 112, 42–66. <https://doi.org/10.1016/j.earscirev.2012.02.001>.

614 Guzzetti, F., Peruccacci, S., Rossi, M., Stark, C.P., 2008. The rainfall intensity-duration  
615 control of shallow landslides and debris flows: An update. *Landslides* 5, 3–17.  
616 <https://doi.org/10.1007/s10346-007-0112-1>.

617 Guzzetti, F., Reichenbach, P., Cardinali, M., Galli, M., Ardizzone, F., 2005.  
618 Probabilistic landslide hazard assessment at the basin scale. *Geomorphology* 72,  
619 272–299. <https://doi.org/10.1016/j.geomorph.2005.06.002>.

620 Haque, U., da Silva, P.F., Devoli, G., Pilz, J., Zhao, B., Khaloua, A., Wilopo, W.,  
621 Andersen, P., Lu, P., Lee, J., Yamamoto, T., Keellings, D., Wu, J., Glass, G.E.,  
622 2019. The human cost of global warming : Deadly landslides and their triggers  
623 (1995-2014). *Sci. Total Environ.* 682, 673–684.  
624 <https://doi.org/10.1016/j.scitotenv.2019.03.415>.

625 Hong, Y., Adler, R.F., 2008. Predicting global landslide spatiotemporal distribution:  
626 Integrating landslide susceptibility zoning techniques and real-time satellite  
627 rainfall estimates. *Int. J. Sediment Res.* 23, 249–257.  
628 [https://doi.org/10.1016/S1001-6279\(08\)60022-0](https://doi.org/10.1016/S1001-6279(08)60022-0).

629 Hong, Y., Adler, R. F., Huffman, G., 2007a. Use of satellite remote sensing data in the

630 mapping of global landslide susceptibility. *Nat. Hazards* 43, 245–256.  
631 <https://doi.org/10.1007/s11069-006-9104-z>.

632 Hong, Y., Adler, R.F., Huffman, G., 2007b. An experimental global prediction system  
633 for rainfall-triggered landslides using satellite remote sensing and geospatial  
634 datasets. *IEEE Trans. Geosci. Remote Sens.* 45, 1671–1680.  
635 <https://doi.org/10.1109/TGRS.2006.888436>.

636 Hong, Y., Alder, R. F., Huffman, G., 2006. Evaluation of the potential of NASA multi-  
637 satellite precipitation analysis in global landslide hazard assessment. *Geophys.*  
638 *Res. Lett.* 33, 1–5. <https://doi.org/10.1029/2006GL028010>.

639 Huang, Y., Zhao, L., 2018. Review on landslide susceptibility mapping using support  
640 vector machines. *Catena* 165, 520-529.  
641 <https://doi.org/10.1016/j.catena.2018.03.003>.

642 Hungr, O., 2007. Dynamics of rapid landslides, in: Sassa, K., Fukuoka, H., Wang, F.,  
643 Wang, G. (Eds.), *Progress in landslide science*. Springer, Berlin, Heidelberg, pp.  
644 47–57. [https://doi.org/10.1007/978-3-540-70965-7\\_4](https://doi.org/10.1007/978-3-540-70965-7_4).

645 Jacobs, L., Kervyn, M., Reichenbach, P., Rossi, M., Marchesini, I., Alvioli, M., Dewitte,  
646 O., 2020. Regional susceptibility assessments with heterogeneous landslide  
647 information: Slope unit- vs. pixel-based approach. *Geomorphology* 356, 107084.  
648 <https://doi.org/10.1016/j.geomorph.2020.107084>.

649 Jarvis, A., Reuter, H., Nelson, A., Guevara, E., 2008. Hole-filled SRTM for the globe.  
650 CGIAR-CSI, v4. Available: <http://srtm.csi.cgiar.org> (accessed 18 December  
651 2020).

652 Jia, G., Tang, Q., Xu, X., 2020. Evaluating the performances of satellite-based rainfall  
653 data for global rainfall-induced landslide warnings. *Landslides* 17, 283–299.  
654 <https://doi.org/10.1007/s10346-019-01277-6>.

655 Juang, C.S., Stanley, T.A., Kirschbaum, D.B., 2019. Using citizen science to expand  
656 the global map of landslides : Introducing the Cooperative Open Online Landslide  
657 Repository ( COOLR ). PLoS One 14, 1–28.  
658 <https://doi.org/10.1371/journal.pone.0218657>.

659 Kirschbaum, D.B., Adler, R. F., Hong, Y., Hill, S., Lerner-Lam, A., 2010. A global  
660 landslide catalog for hazard applications: Method, results, and limitations. Nat.  
661 Hazards 52, 561–575. <https://doi.org/10.1007/s11069-009-9401-4>.

662 Kirschbaum, D.B., Adler, R. F., Hong, Y., Lerner-Lam, A., 2009. Evaluation of a  
663 preliminary satellite-based landslide hazard algorithm using global landslide  
664 inventories. Nat. Hazards Earth Syst. Sci. 9, 673–686.  
665 <https://doi.org/10.5194/nhess-9-673-2009>.

666 Kirschbaum, D.B., Stanley, T., 2018. Satellite-Based Assessment of Rainfall-Triggered  
667 Landslide Hazard for Situational Awareness. Earth's Futur. 6, 505–523.  
668 <https://doi.org/10.1002/2017EF000715>.

669 Kirschbaum, D.B., Stanley, T., Zhou, Y., 2015. Spatial and temporal analysis of a  
670 global landslide catalog. Geomorphology 249, 4–15.  
671 <https://doi.org/10.1016/j.geomorph.2015.03.016>.

672 Li, W., Liu, C., Hong, Y., Zhang, X., Wang, Z., Saharia, M., Sun, W., Yao, D., Chen,  
673 W., Chen, S., Yang, X., Yue, J., 2016. A public Cloud-based China's Landslide  
674 Inventory Database (CsLID): development, zone, and spatiotemporal analysis for  
675 significant historical events, 1949-2011. J. Mt. Sci. 13, 1275–1285.  
676 <https://doi.org/10.1107/s11629-015-3659-7>.

677 Lin, L., Lin, Q., Wang, Y., 2017. Landslide susceptibility mapping on a global scale  
678 using the method of logistic regression. Nat. Hazards Earth Syst. Sci. 17, 1411–  
679 1424. <https://doi.org/10.5194/nhess-17-1411-2017>.

680 Marchesini, I., Ardizzone, F., Alvioli, M., Rossi, M., Guzzetti, F., 2014. Non-  
681 susceptible landslide areas in Italy and in the Mediterranean region. *Nat. Hazards*  
682 *Earth Syst. Sci.* 14, 2215–2231. <https://doi.org/10.5194/nhess-14-2215-2014>.

683 Mazengarb, C., Stevenson, M., 2010. *Tasmanian Landslide Map Series: User Guide*  
684 *and Technical Methodology*. Tasmanian Geological Survey, Technical report.  
685 [https://www.mrt.tas.gov.au/mrtdoc/dominfo/download/UR2010\\_01/UR2010\\_01.](https://www.mrt.tas.gov.au/mrtdoc/dominfo/download/UR2010_01/UR2010_01.pdf)  
686 pdf.

687 McKeon, C., 2016. *National Landslide Susceptibility Mapping Project Summary*.  
688 Geological Survey Ireland, Technical report.  
689 [https://www.gsi.ie/documents/National\\_Sus\\_Map\\_Summary\\_FINAL\\_NEW.pdf](https://www.gsi.ie/documents/National_Sus_Map_Summary_FINAL_NEW.pdf).

690 Nadim, F., Jaedicke, C., Smebye, H., Kalsnes, B., 2013. Assessment of global landslide  
691 hazard hotspots, in: Sassa, K., Rouhban, B., Briceno, S., McSaveney, M., He, B.  
692 (Eds.), *Landslides: Global Risk Preparedness*. Springer-Verlag, Berlin,  
693 Heidelberg, pp. 59–71. [https://doi.org/10.1007/978-3-642-22087-6\\_4](https://doi.org/10.1007/978-3-642-22087-6_4).

694 Nadim, F., Kjekstad, O., Peduzzi, P., Herold, C., Jaedicke, C., 2006. Global landslide  
695 and avalanche hotspots. *Landslides* 3, 159–173. [https://doi.org/10.1007/s10346-](https://doi.org/10.1007/s10346-006-0036-1)  
696 006-0036-1.

697 Osuchowski, M., Atkinson, R., 2008. Connecting diverse landslide inventories for  
698 improved information in Australia. *Proceedings of the 1st World Landslide Forum*,  
699 Tokyo, Japan, 18–21 November 2008.

700 Peruccacci, S., Brunetti, M.T., Gariano, S.L., Melillo, M., Rossi, M., Guzzetti, F., 2017.  
701 Rainfall thresholds for possible landslide occurrence in Italy. *Geomorphology* 290,  
702 39–57. <https://doi.org/10.1016/j.geomorph.2017.03.031>.

703 Petley, D., Froude, M., 2019. *Guide to the Global Fatal Landslide Database on ArcGIS*  
704 Online (version 2). Available:

705 <https://drive.google.com/drive/folders/1kxUSXB110HPrGXIur6bM4PBoKX0C>  
706 [\\_LY](#) (accessed 18 December 2020).

707 Reichenbach, P., Rossi, M., Malamud, B.D., Mihir, M., Guzzetti, F., 2018. A review of  
708 statistically-based landslide susceptibility models. *Earth-Science Rev.* 180, 60–91.  
709 <https://doi.org/10.1016/j.earscirev.2018.03.001>.

710 Reuter, H., Nelson, A., Jarvis, A., 2007. An evaluation of void filling interpolation  
711 methods for SRTM data. *Int. J. Geogr. Inf. Sci.* 21, 983–1008.  
712 <https://doi.org/10.1080/13658810601169899>.

713 Rickenmann, D., 2005. Runout prediction methods, in: Jakob, M., Hungr, O. (Eds.),  
714 Debris-flow Hazards and Related Phenomena. Springer, Berlin, Heidelberg, pp.  
715 305–324. [https://doi.org/10.1007/3-540-27129-5\\_13](https://doi.org/10.1007/3-540-27129-5_13).

716 Rosser, B., Dellow, S., Haubrock, S., Glassey, P., 2017. New Zealand’s national  
717 landslide database. *Landslides* 14, 1949–1959. [https://doi.org/10.1007/s10346-](https://doi.org/10.1007/s10346-017-0843-6)  
718 [017-0843-6](https://doi.org/10.1007/s10346-017-0843-6). Sayre, R., Frye, C., Karagulle, D., Krauer, J., Breyer, S., Aniello, P.,  
719 Wright, D.J., Payne, D., Adler, C., Warner, H., VanSistine, D.P., Cress, J., 2018.  
720 A New High-Resolution Map of World Mountains and an Online Tool for  
721 Visualizing and Comparing Characterizations of Global Mountain Distributions.  
722 *Mt. Res. Dev.* 38, 240–249. <https://doi.org/10.1659/mrd-journal-d-17-00107.1>.

723 Slaughter, S.L., Burns, W.J., Mickelson, K.A., Jacobacci, K.E., Biel, A., Contreras,  
724 T.A., 2017. Protocol for landslide inventory mapping from lidar data in  
725 Washington state. *Washington Geological Survey Bulletin* 82.  
726 [http://www.dnr.wa.gov/Publications/ger\\_b82\\_landslide\\_inventory\\_mapping\\_pro](http://www.dnr.wa.gov/Publications/ger_b82_landslide_inventory_mapping_protocol.zip)  
727 [tocol.zip](http://www.dnr.wa.gov/Publications/ger_b82_landslide_inventory_mapping_protocol.zip).

728 Stanley, T., Kirschbaum, D.B., 2017. A heuristic approach to global landslide  
729 susceptibility mapping. *Nat. Hazards* 87, 145–164.

730 <https://doi.org/10.1007/s11069-017-2757-y>.

731 Tanyas, H., Lombardo, L., 2020. Completeness Index for Earthquake-Induced  
732 Landslide Inventories. *Eng. Geol.* 264, 105331.  
733 <https://doi.org/10.1016/j.enggeo.2019.105331>.

734 Tanyas, H., Rossi, M., Alvioli, M., van Westen, C.J., Marchesini, I., 2019a. A global  
735 slope unit-based method for the near real-time prediction of earthquake-induced  
736 landslides. *Geomorphology* 327, 126–146.  
737 <https://doi.org/10.1016/j.geomorph.2018.10.022>.

738 Tanyas, H., van Westen, C.J., Persello, C., Alvioli, M., 2019b. Rapid prediction of the  
739 magnitude scale of landslide events triggered by an earthquake. *Landslides* 16,  
740 661–676. <https://doi.org/10.1007/s10346-019-01136-4>.

741 Trigila, A., Iadanza, C., Spizzichino, D., 2010. Quality assessment of the Italian  
742 Landslide Inventory using GIS processing. *Landslides* 7, 455–470.  
743 <https://doi.org/10.1007/s10346-010-0213-0>.

744 UGS, 2018. Landslides and Debris Flows. Utah Geological Survey. Available:  
745 <https://gis.utah.gov/data/geoscience/landslides/>(accessed 18 December 2020).

746 USGS, 2020. Landslide Hazards. United States Geological Survey. Available:  
747 <https://www.usgs.gov/natural-hazards/landslide-hazards> (accessed 18 December  
748 2020).

749 Van Den Eeckhaut, M., Hervás, J., 2012. State of the art of national landslide databases  
750 in Europe and their potential for assessing landslide susceptibility, hazard and risk.  
751 *Geomorphology* 139-140, 545-558.  
752 <https://doi.org/10.1016/j.geomorph.2011.12.006>.

753 Van Den Eeckhaut, M., Hervás, J., Jaedicke, C., Malet, J.P., Montanarella, L., Nadim,  
754 F., 2012. Statistical modelling of Europe-wide landslide susceptibility using

755 limited landslide inventory data. *Landslides* 9, 357–369.  
756 <https://doi.org/10.1007/s10346-011-0299-z>.

757 WGS, 2020. Landslide protocol inventory mapping--GIS data, February, 2020.  
758 Washington Geological Survey Digital Data Series 19, version 2.0.  
759 [https://fortress.wa.gov/dnr/geologydata/publications/data\\_download/ger\\_portal\\_1](https://fortress.wa.gov/dnr/geologydata/publications/data_download/ger_portal_1)  
760 [andslide\\_inventory.zip](https://fortress.wa.gov/dnr/geologydata/publications/data_download/ger_portal_1).

761 Wilde, M., Günther, A., Reichenbach, P., Malet, J.P., Hervás, J., 2018. Pan-European  
762 landslide susceptibility mapping: ELSUS version 2. *J. Maps* 14, 97–104.  
763 <https://doi.org/10.1080/17445647.2018.1432511>.

764 YNDPMC, 2016. Yearbook of disaster prevention and mitigation in Yunnan, China.  
765 Yunnan Disaster Prevention and Mitigation Committee, Technical report.  
766 [http://ss.zhizhen.com/detail\\_38502727e7500f268f2766febf6686c44c842e57df45](http://ss.zhizhen.com/detail_38502727e7500f268f2766febf6686c44c842e57df45)  
767 [19051921b0a3ea25510134114c969f2eae5cd616e9cc3373a273a0e2ec07cd17b56](http://ss.zhizhen.com/detail_38502727e7500f268f2766febf6686c44c842e57df45)  
768 [351cc4e29623d58fdb5465aecc36b7b3bbd319923364c989b?](http://ss.zhizhen.com/detail_38502727e7500f268f2766febf6686c44c842e57df45).

769

770 **Tables and Figures**

771 **Table 1.** Summary information of global (1-2), national (3-9) and regional (10-18)

772 landslide datasets. Region: the geographical extent of datasets, the two global datasets

773 are labeled by the name of datasets. Type: features of landslide data. Record (O):

774 number of landslide records in the original datasets. Record (S): selected number of

775 landslide records with high accuracy in each dataset. Area: area of region, from wiki

776 pages (accessed on December 18, 2020).  $N_L$ : number of landslide records per  $10^3 \text{ km}^2$ .

#	Region	Extent	Type	Record (O)	Record (S)	Area ( $10^3 \text{ km}^2$ )	$10^3 N_L$ ( $\text{km}^{-2}$ )	Reference
1	COOLR	global	point	12,685	3,377	--	--	Juang et al., 2019
2	GFLD	global	polygon	5,490	297	--	--	Petley and Froude, 2019
3	Australia	national	point	1,974	274	7,692	0.04	Geoscience Australia, 2012
4	China	national	point	990	815	9,597	0.08	Li et al., 2016
5	Ireland	national	point	2,778	855	84	10.18	McKeon, 2016
6	Ireland	national	polygon	1,417	736	84	8.76	McKeon, 2016
7	Italy	national	point	4,934	3,195	301	10.61	Calvello and Pecoraro, 2018
8	New Zealand	national	point	19,030	5,789	268	21.60	Rosser et al., 2017
9	Turkey	national	point	389	317	783	0.40	Görüm and Fidan, 2021
10	Arizona, USA	regional	polygon	6,374	3,717	295	12.60	AGS, 2015
11	Guangdong, China	regional	point	1,491	781	180	4.34	GDDPMC, 2016
12	Oregon, USA	regional	point	13,994	2,807	98	28.64	Burns and Madin, 2009
13	Oregon, USA	regional	polygon	44,929	5,957	98	60.79	Burns and Madin, 2009
14	Tasmania, Australia	regional	point	3,266	764	68	11.24	Mazengarb and Stevenson, 2010
15	Utah, USA	regional	polygon	25,589	1,722	220	7.83	UGS, 2018
16	Vermont, USA	regional	point	2,731	352	25	14.08	Cliff and Springston, 2012
17	Washington, USA	regional	polygon	45,297	7,650	185	41.35	WGS, 2020
18	Yunnan, China	regional	point	453	203	394	0.52	YNDPMC, 2016

777

778 **Table 2.** Validation results of the proposed quantile non-linear (QNL) non-  
779 susceptibility model by Marchesini et al. (2014) for different landslide types based on  
780 all the landslide data of eighteen datasets (in Table 1). About 31% of the landslides  
781 include type information. False positives (*FP*): number of landslides below the QNL  
782 threshold curve (in non-susceptible area).

Landslide type	False positives ( <i>FP</i> )	Total number of landslides ( <i>TN+FP</i> )	False positive rate ( <i>FPR</i> )
Flow	31	570	0.05
Fall	85	973	0.09
Slide	130	1,197	0.11
Complex	107	1,029	0.10
Debris flow	271	1,507	0.18
Earth flow	83	921	0.09
Translational/ rotational slide	185	2,079	0.09
Mudslide	90	773	0.12
Earth slide	763	3,302	0.23
(undefined)	2,884	27,257	0.11
Total	4,629	39,608	0.12

783  
784

785 **Table 3.** Comparison between the lowest susceptibility class in global and continental  
 786 susceptibility maps and non-susceptible class in our global landslide non-susceptibility  
 787 map (Figure 5a).

Extent	Susceptibility map	Non-susceptible area in “very low” class
Global	Giuliani and Peduzzi, 2011	86.0%
	Stanley and Kirschbaum, 2017	99.4%
	Lin et al., 2017	89.0%
	(Average)	91.5%
Africa	Broeckx et al., 2018	97.8%
Europe	Wilde et al., 2018	99.2%

788

789 **Table 4.** Statistics of population and human settlement in non-susceptible and “not non-  
 790 susceptible” areas in a quasi-global scale.

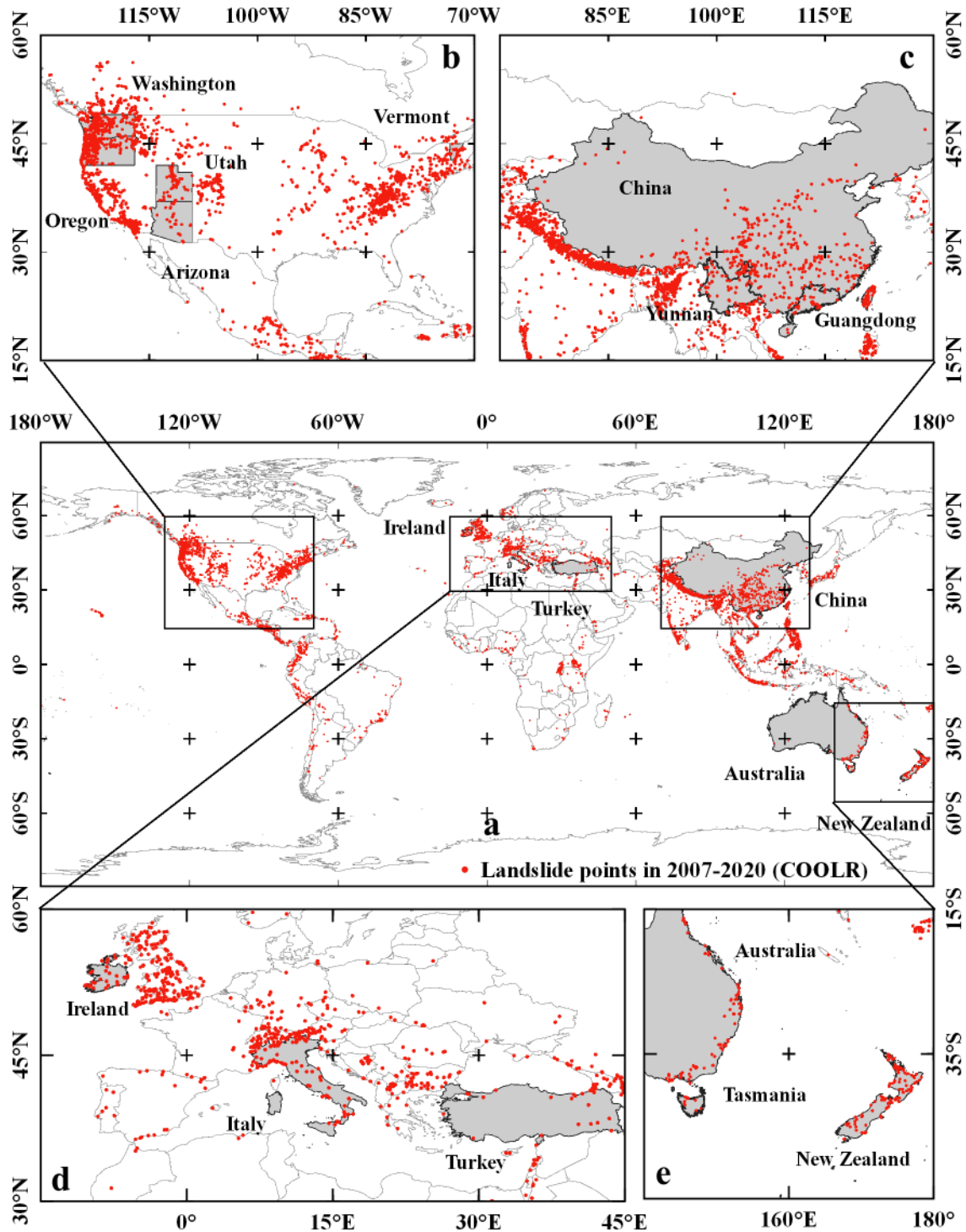
791

	Not non- susceptible area	Non-susceptible area	Total
Area ( $10^6$ km <sup>2</sup> )	20.1	96.9	116.9
Percentage of area	17.1%	82.9%	100.0%
Built-up area ( $10^3$ km <sup>2</sup> )	67.5	701.3	768.8
Percentage of built-up area	8.8%	91.2%	100.0%
Built-up density	0.3%	0.7%	0.6%
Population ( $10^6$ )	594	6,632	7,226
Percentage of population	8.2%	91.8%	100.0%
Population density (km <sup>-2</sup> )	29.6	68.2	61.6

792 **Table 5.** Parameters of QNL models for the globe and different regions corresponding  
793 to regional views in Figure 1 and landslide types based on COOLR datasets. The model  
794 is defined as Eq. (1) in Section 3.1. Datasets: Region B (grouped datasets in Fig. 1b),  
795 Region C (grouped datasets in Fig. 1c), Region D (grouped datasets in Fig. 1d), Region  
796 E (grouped datasets in Fig. 1e).

	Dataset	$\alpha$	$\beta$
Regions	COOLR	1.938	0.0030
	Region B	2.326	0.0026
	Region C	1.246	0.0036
	Region D	1.431	0.0036
	Region E	3.686	0.0029
Landslide types	Debris flows	1.725	0.0033
	Translational/ rotational slides	3.800	0.0022
	Mudslides	1.796	0.0035
	Rock falls	3.521	0.0024
	Complex landslides	2.686	0.0029
	Others	1.846	0.0030

797



798

799

**Fig. 1.** Geographic (administrative) extents of available regional landslide datasets, of

800

which six are national datasets labeled in **a**, in this analysis. Points in red represent

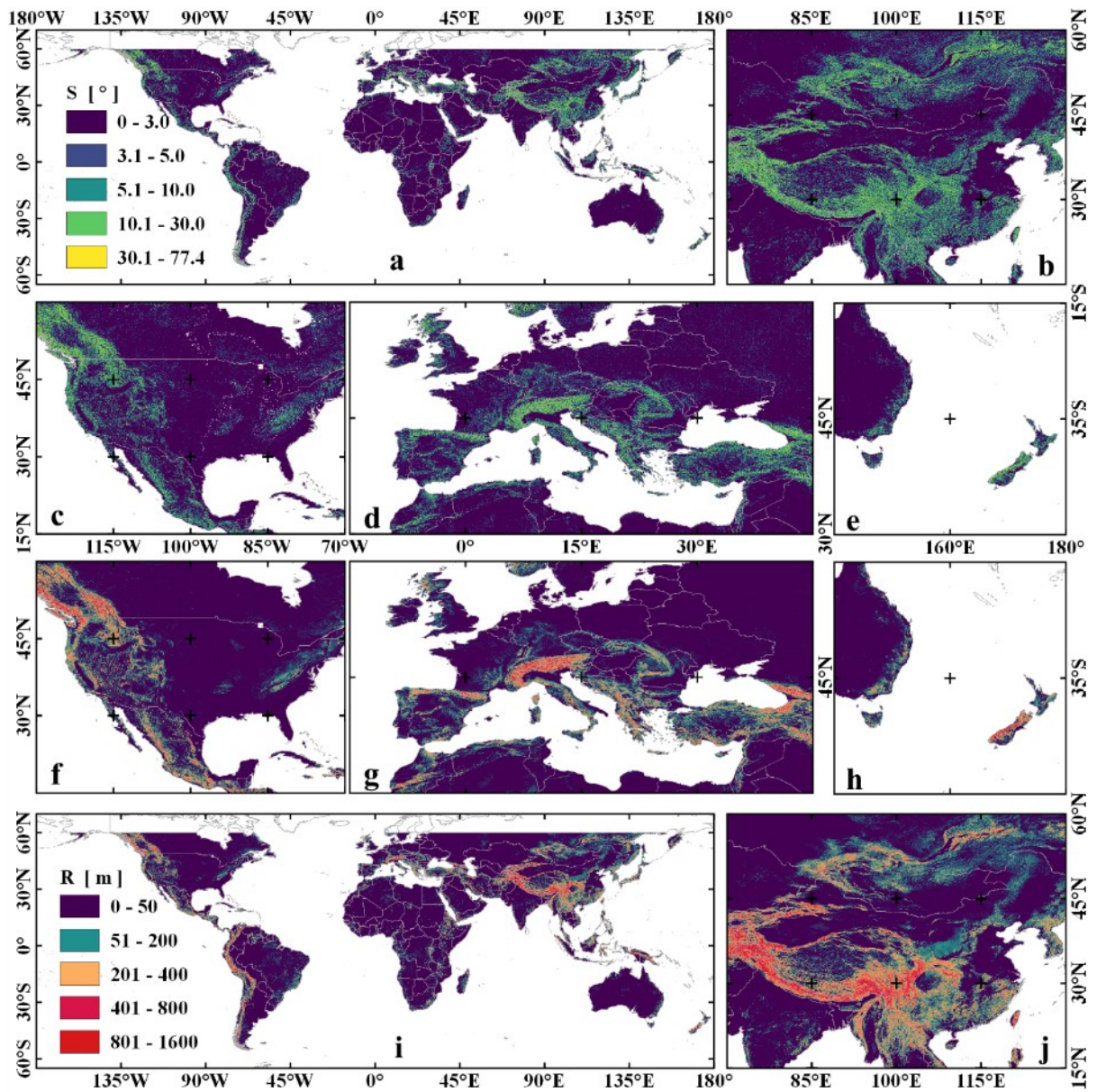
801

landslide locations (12,685 points) in a global dataset (COOLR). Regional views (**b-e**)

802

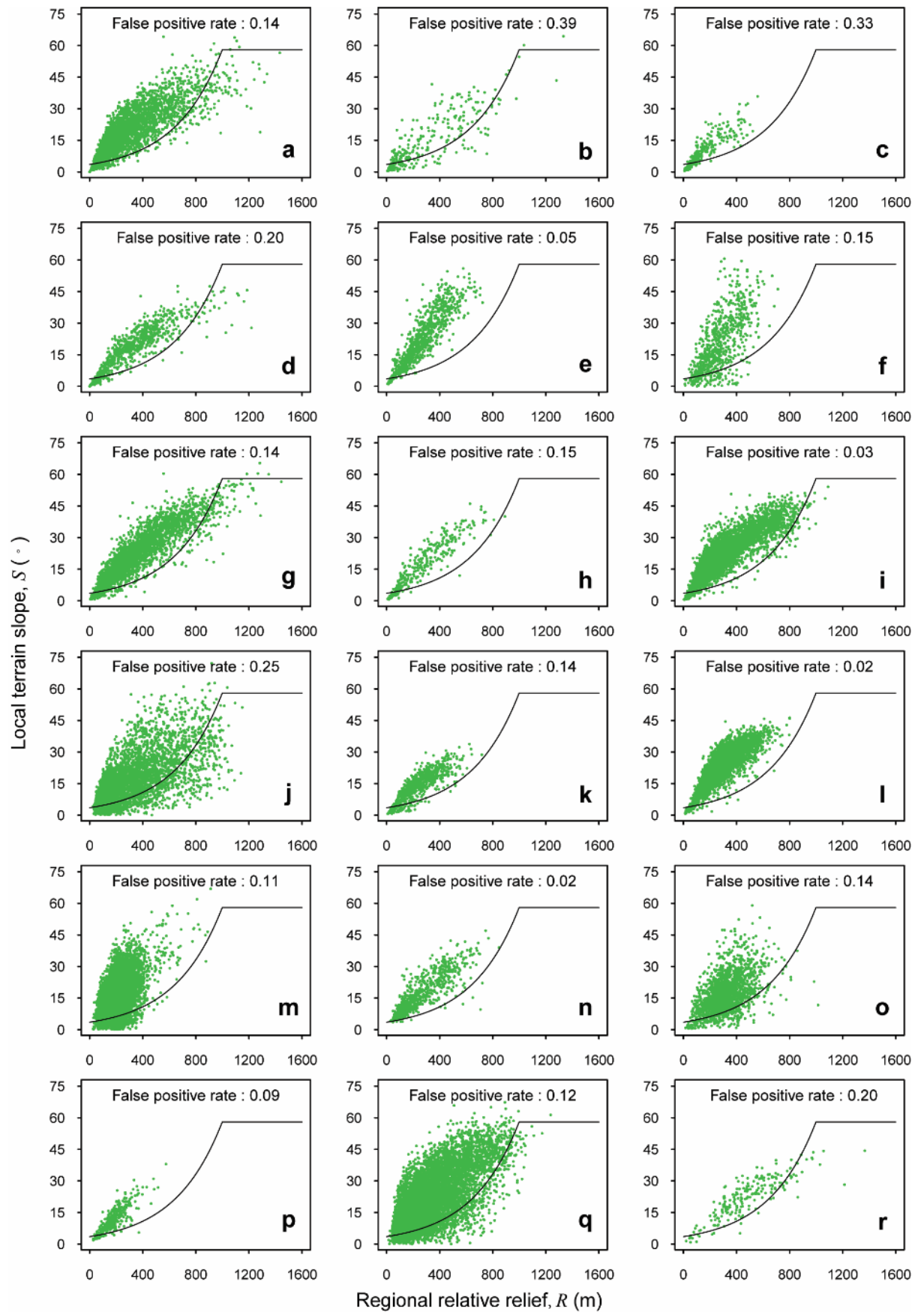
show four groups of the datasets.

803



804  
 805 **Fig. 2.** Global maps of local terrain slope,  $S$  (a) and regional relative relief,  $R$  (i) based  
 806 on the  $\sim 90$ -m SRTM DEM elevation data. Regional maps are shown to provide the  
 807 enlarged view corresponding to that in Figure 1, *i.e.*, most of the Asia (b, j), most of  
 808 the North America (c, f), Mediterranean region and its surroundings (d, g), and the  
 809 eastern Australia and New Zealand (e, h).

810



811

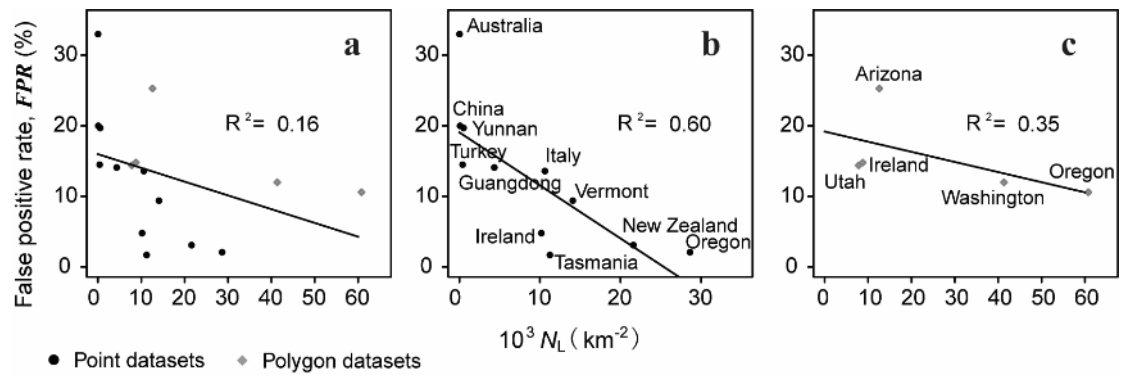
812 **Fig. 3.** Validation results for available global and regional landslide datasets (Table 1).

813

Green points represent the regional relative relief and local terrain slope corresponding

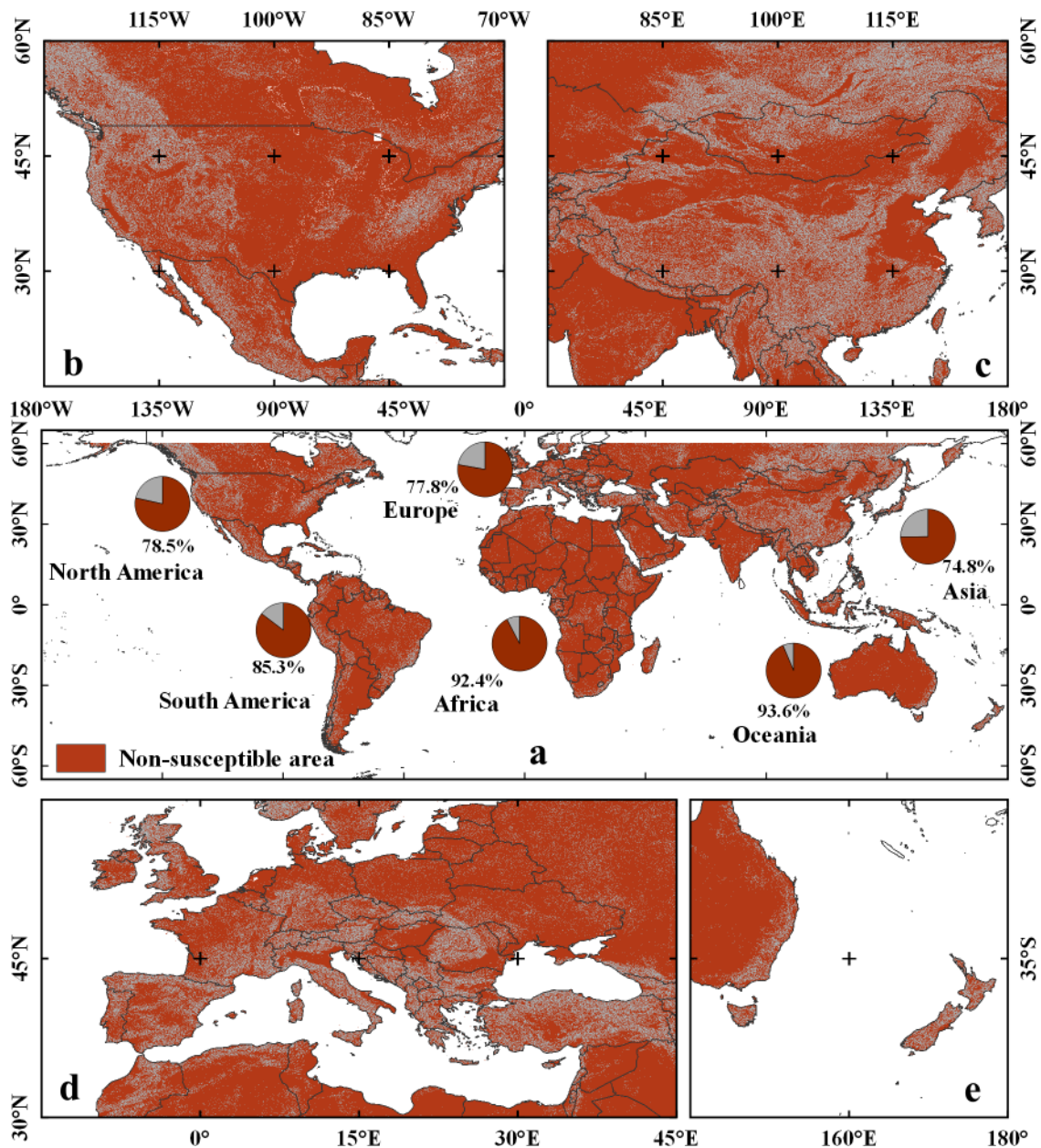
814 to each landslide feature, and black curves the quantile non-linear (QNL) non-  
815 susceptibility threshold curve (Eq. 1). Landslide datasets: **(a)** COOLR, **(b)** GFLD, **(c)**  
816 Australia, **(d)** China, **(e)** Ireland (point features), **(f)** Ireland (polygon features), **(g)** Italy,  
817 **(h)** Turkey, **(i)** New Zealand, **(j)** Arizona, USA, **(k)** Guangdong, China, **(l)** Oregon,  
818 USA (point features), **(m)** Oregon, USA (polygon features), **(n)** Tasmania, Australia,  
819 **(o)** Utah, USA, **(p)** Vermont, USA, **(q)** Washington, USA, **(r)** Yunnan, China. False  
820 positive rate (*FPR*) is the ratio of the number of landslides below the threshold curve  
821 (false positives, *FP*) over the total number of landslides (*FP* and true negatives, *TN*) in  
822 each dataset.

823



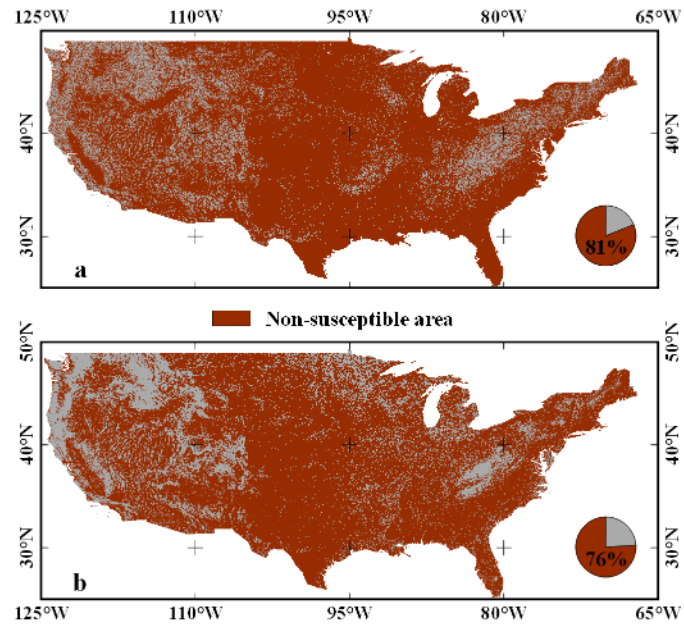
825 **Fig. 4.** Relationship between the landslide density ( $N_L$  represents the number of  
826 reported landslides per  $10^3 \text{ km}^2$  in Table 1) and  $FPR$  for regional landslide datasets in  
827 Figure 3: (a) point and polygon datasets, (b) point datasets, (c) polygon datasets. Black  
828 curves are linear fits.

829



830  
831 **Fig. 5.** A global map of landslide non-susceptibility in ~90-m resolution (a) based on  
832 QNL model proposed by Marchesini et al. (2014) in Section 3.1, and percentages of  
833 non-susceptible areas in each continent. Landmass outside the non-susceptible areas is  
834 shown in light gray. Non-susceptible areas are also mapped in regions corresponding  
835 to that in Figure 1, *i.e.*, most of the North America (b), most of the Asia (c),  
836 Mediterranean region and its surroundings (d), and the eastern Australia and New  
837 Zealand (e).

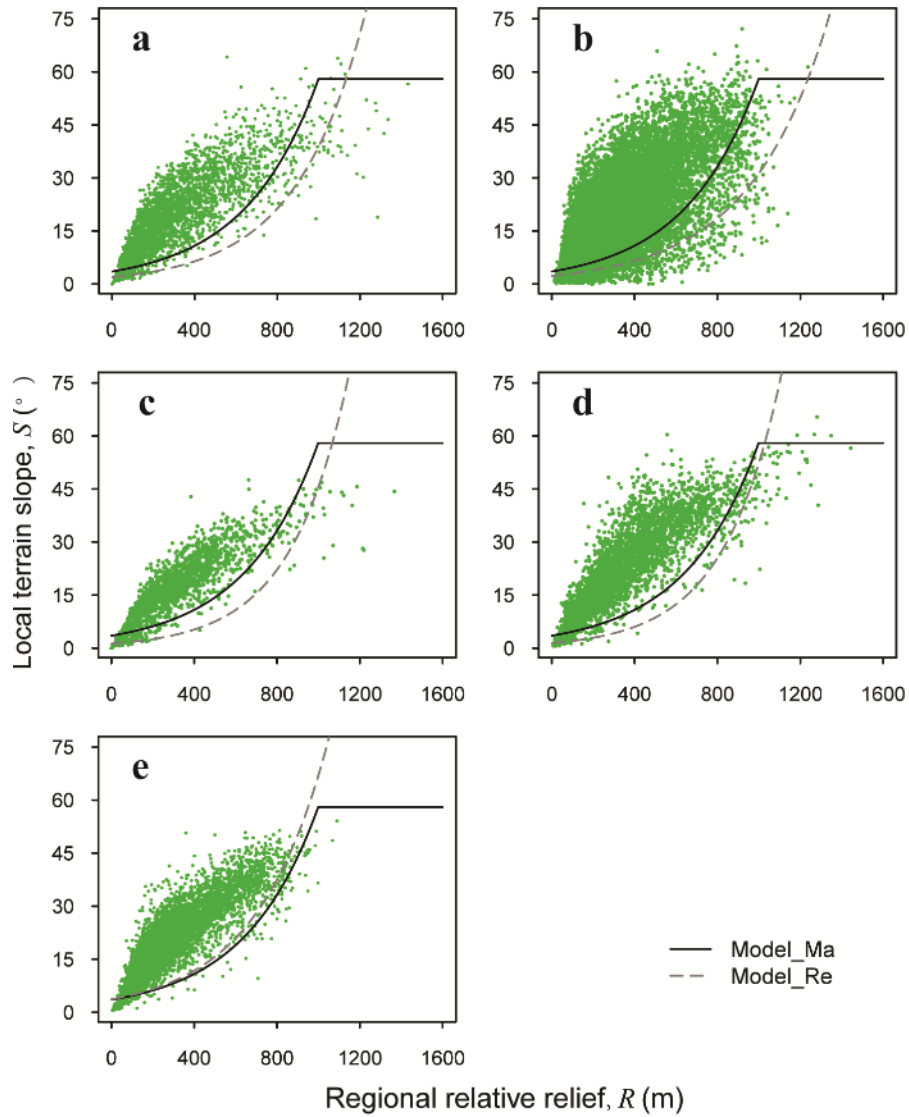
838



839

840 **Fig. 6.** Non-susceptibility maps (~90 m) in the conterminous United States based on  
 841 the QNL model (a) proposed by Marchesini et al. (2014) and the linear model (b)  
 842 proposed by Godt et al. (2012). Landmasses outside the non-susceptible areas is shown  
 843 in light gray.

844



845  
 846 **Fig. 7.** Regional QNL non-susceptibility models based on the groups of landslide  
 847 datasets. Model\_Ma: QNL model proposed by Marchesini et al. (2014). Model\_re:  
 848 regional QNL models for (a) COOLR dataset, (b) Region B (grouped datasets in Fig.  
 849 1b), (c) Region C (grouped datasets in Fig. 1c), (d) Region D (grouped datasets in Fig.  
 850 1d), and (e) Region E (grouped datasets in Fig. 1e).  
 851

